Thin Solid Films 539 (2013) 303–308

Contents lists available at SciVerse ScienceDirect

Thin Solid Films

journal homepage: www.elsevier.com/locate/tsf

Manipulating structure and enhancing conductivity of polymer acid doped polyaniline by exploiting redox chemistry

Jacob Tarver *, Yueh-Lin Loo *

Department of Chemical and Biological Engineering, Princeton University, Princeton, NJ 08544, USA

ARTICLE INFO

Article history:
Received 20 December 2012
Received in revised form 10 May 2013
Accepted 10 May 2013
Available online 22 May 2013

Keywords:
Polyaniline
Conducting polymers
Conductivity enhancement
Chemical redox reaction

ABSTRACT

By reversibly accessing the oxidation states of polyaniline that is template synthesized on poly(2-acrylamido-2-methyl-1-propanesulfonic acid), extensive structural relaxations are induced that result in significant conductivity enhancement. The electrostatic interactions between polyaniline and its template can be neutralized through chemical reduction with hydrazine monohydrate, after which the polymer acid can be plasticized by water vapor to drive structural relaxation. Exposure to nitric oxide leads to re-oxidation of polyaniline and concurrent reassociation with its polymer acid dopant. Following this redox cycling process, the conductivity of polyaniline films increases from 0.4 S/cm to as high as 11 S/cm. This enhancement is attributed to the same extensive polymer chain relaxation and the simultaneous elimination of the particulate nature of template-synthesized polyaniline previously described following solvent annealing in dichloroacetic acid. While solvent annealing also increases the conductivity of films comprising commercially available poly(3,4-ethylenedioxythiophene):poly(styrene sulfonic acid), redox cycling induces no improvement in the electrical conductivity of such films. This difference suggests that conductivity enhancement in poly(3,4-ethylenedioxythiophene) films through solvent annealing stems from a mechanism markedly different from the structural relaxation responsible for improving the electrical properties of polymer acid-doped polyaniline, and likely results from the physical removal of an insulating poly(styrene sulfonic acid) overlayer.

1. Introduction

Water-dispersible particles comprising polymer-acid-doped conducting polymers have emerged as high performance materials in a number of applications [1–4]. Films cast from aqueous dispersions of poly(3,4-ethylenedioxythiophene):poly(styrene sulfonic acid), or PEDOT:PSS, are widely used as hole-transport layers in the study of organic optoelectronic devices, such as light-emitting diodes and photovoltaic cells; [2,3] films cast from dispersions of polyaniline (PANI) template-polymerized on poly(2-acrylamido-2-methyl-1-propanesulfonic acid), or PAAMPSA, meanwhile, show outstanding promise as active materials in electrochromic research [4–9]. A growing volume of literature has described the strong influence of synthesis and processing conditions over the properties of these materials [10]. Manipulating the molecular weight and molecular weight distribution of PAAMPSA prior to the template-synthesis of PANI, for instance, permits tunability of the size and size distribution, respectively, of the resulting PANI–PAAMPSA particles [11–13]. Because the electrical conductivity of PANI–PAAMPSA films increases with decreasing particle size, moderating PAAMPSA's molecular characteristics allows direct and rigorous control over PANI–PAAMPSA's electrical properties [13].

Following synthesis of the particles, the electrical and optical properties of films comprising either PANI–PAAMPSA or PEDOT:PSS can be further modified through a number of post-deposition processing techniques involving the addition of, or annealing in, secondary solvents [14–18]. Many of these treatments have reported to render PEDOT:PSS films significantly more conductive than those cast from the original aqueous dispersions. Mixing sorbitol or ethylene glycol with PEDOT:PSS prior to deposition, for instance, enhances the conductivity of thin films from 0.2 S/cm to 48 and 200 S/cm, respectively [15,18]. Alternatively, aggressive agitation in dichloroacetic acid (DCA) at 100 °C increases the electrical conductivity of PANI–PAAMPSA films from 0.4–2.4 S/cm to 40 S/cm, and that of PEDOT:PSS films to as high as 200 S/cm [2].

The mechanisms for these enhancements, however, are not well understood. Although DCA treatment induces dramatic increases in the conductivity of both PANI–PAAMPSA and PEDOT:PSS, structural characterization suggests that this secondary solvents act on PANI–PAAMPSA and PEDOT:PSS films through disparate routes [2]. For instance, the surface of DCA-treated PANI–PAAMPSA films smoothens dramatically relative to the surface of as-spun films, while the surface structure of PEDOT:PSS films undergoes a slight roughening [2]. DCA is speculated to interrupt the doping interactions between PANI and PAAMPSA, and subsequently plasticize and relax the liberated PAAMPSA prior to solvent evaporation, thereby imparting significant structural change [2]. Alternatively, conductivity enhancement in

* Corresponding authors. Tel.: +1 609 258 9091; fax: +1 609 258 0211.
E-mail addresses: jacob.tarver@nist.gov (J. Tarver), lloo@princeton.edu (Y.-L. Loo).

0040-6090/$ – see front matter © 2013 Elsevier B.V. All rights reserved.
http://dx.doi.org/10.1016/j.tsf.2013.05.081

PEDOT:PSS following solvent annealing is speculated to stem from the removal of a thin insulating overlayer of PSS that forms upon spin casting given the solvation of PSS in DCA and other solvents [14,16].

To better understand the mechanistic differences between conductivity enhancement in polymer acid-doped conductive polymers, the influence of redox chemistry on the structural, optical, and electrical properties of PANI–PAAMPSA and PEDOT:PSS is explored in this paper. By chemically reducing PANI from its electrically conductive emeraldine salt (ES) form to its neutral leucoemeraldine base (LB) oxidation state, as shown in Scheme 1a, its electrostatic interactions with PAAMPSA can be eliminated. After allowing the liberated PAAMPSA to relax *via* plasticization by moisture, PANI can be reoxidized and its electrostatic interactions with PAAMPSA reestablished, as shown in Scheme 1b. By tracking changes in structural, optical, and electrical properties as PANI–PAAMPSA is chemically reduced then oxidized, we conclusively show that structural relaxation is the dominant mechanism behind its conductivity improvement. Conversely, by assessing the structural, optical, and electrical response of PEDOT:PSS under identical conditions, we show that, conductivity enhancement in PEDOT:PSS must stem from a distinctly different mechanism.

2. Experimental details

PANI–PAAMPSA was synthesized *via* previously described procedures [12]. Aqueous solutions of aniline (Fisher Scientific, 99.9%) and PAAMPSA (Scientific Polymer Products, 724 kg/mol poly(ethylene oxide)-equivalent molecular weight, polydispersity index of 1.64) were separately deaerated under nitrogen flow for 30 min in ice baths prior to mixing to prevent uncontrolled initiation of polymerization. An aqueous solution of ammonium peroxydisulfate (APS, Fisher Scientific, 98.9%) was separately deaerated in an ice bath for 30 min prior to injection into the aniline/PAAMPSA solution to initiate PANI–PAAMPSA synthesis. The conditions at the onset of the polymerization were maintained at a 1:1:0.9 molar ratio of aniline:AAMPSA:APS, and an overall aniline concentration of 70 mM. The reaction contents were stirred in an ice bath for 24 h following initiation to permit the reaction to reach completion. Following the reaction, PANI–PAAMPSA was recovered by slowly adding acetone to the contents of the reaction vessel under constant stirring to cause precipitation of the desired product. The supernatant was decanted and the remaining solids were washed under excess acetone prior to drying *in-vacuo* for 24 h. After drying, the resulting PANI–PAAMPSA powder was dispersed at 5 wt.% by stirring continuously for 10–14 days in 18.2 MΩ water deionized using a Milli-Q Academic purification system. Films used in this study were subsequently deposited from this dispersion *via* spin-coating. Film thickness was maintained at 450 nm to minimize pinholes and to ensure film continuity.

Reduction of PANI from its ES to LB oxidation state was accomplished by inverting PANI–PAAMPSA films above Petri dishes containing hydrazine monohydrate (Sigma-Aldrich, 98%). Ultraviolet–visible/near-infrared (UV–vis/NIR) spectroscopy (Agilent 8453) and Fourier transform infrared (FTIR) spectroscopy (Nicolet Magna 860) were used to identify the amount and duration of hydrazine monohydrate exposure necessary to completely reduce PANI–PAAMPSA to its LB state. Films were then slowly dried over a successive series of saturated potassium chloride, sodium chloride, potassium carbonate, potassium acetate, and lithium chloride salt baths to moderate relative humidity and prevent the formation of fissures [19]. Following drying, tapping-mode atomic force microscopy (AFM; Veeco Dimensions Nanoman) was utilized to determine the extent of structural relaxation following hydrazine monohydrate exposure, as quantified by the films' root-mean-square (RMS) roughness. These films were subsequently oxidized by exposure to gaseous nitric oxide (NO); *in-situ* absorbance and conductivity measurements quantified structural rearrangement and conductivity enhancement, respectively, upon oxidation.

Iron sulfate heptahydrate (Fisher Scientific, ≥99%) and sodium nitrite (Fisher Scientific, ≥97%) were reacted aqueously to generate NO according to Reaction (1):

$$6FeSO_{4(aq)} + 12NaNO_{2(aq)} \rightarrow 2Fe_2O_{3(s)} + Fe_2O_3{\cdot}N_2O_{5(aq)} + 10NO_{(g)} + 6Na_2SO_{4(aq)}. \quad (1)$$

To prevent the rapid oxidation of NO to nitrous oxide upon generation, 0.2 M aqueous solutions of iron sulfate heptahydrate and sodium nitrite were prepared separately and thoroughly deaerated under nitrogen prior to mixing. The desired reaction was induced by injecting the iron sulfate heptahydrate solution into a stirred vessel containing the sodium nitrite solution at a 1 mL/min *via* a syringe pump. Nitrogen was then used to deliver the freshly produced NO to PANI–PAAMPSA films. UV–vis/NIR spectroscopy was used to identify the amount and

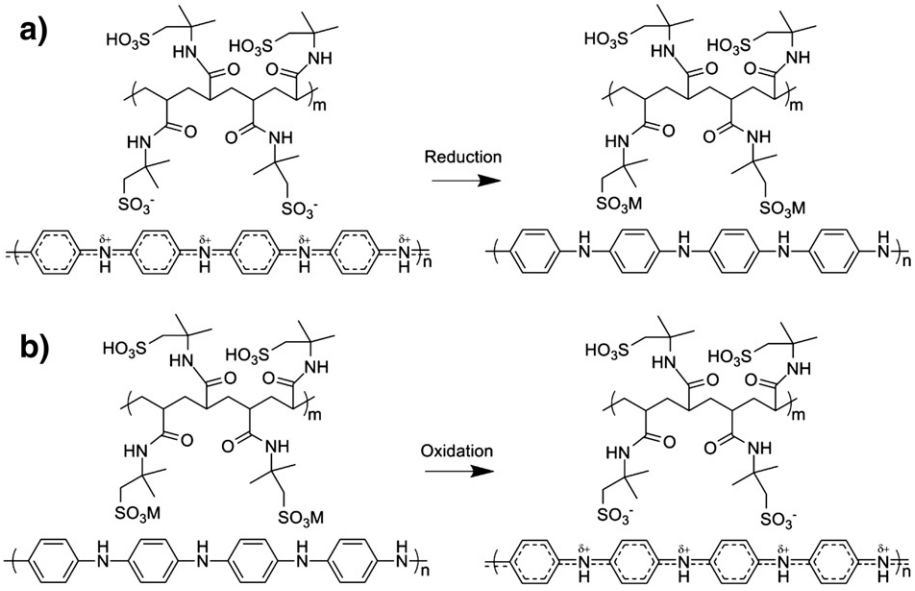

Scheme 1. Proposed reaction sequence for chemical redox-cycling of PANI–PAAMPSA depicted as (a) the reduction of ES to LB under exposure to hydrazine monohydrate vapor, followed by (b) the subsequent oxidation of LB back to ES under exposure to gaseous NO. M represents PAAMPSA's charge-balancing counterion when unassociated with PANI, though successful realization of reaction (b) requires its removal.

duration of NO exposure necessary to oxidize PANI–PAAMPSA from its LB state. A customized UV–vis/NIR cell, was employed to permit simultaneous recording of the changes in the optical absorption and electrical conductivity of PANI–PAAMPSA during exposure. This setup uses films of PANI–PAAMPSA deposited on pre-patterned ITO substrates in which all ITO was etched away with the exception of four rectangular segments extending down 0.5 cm from the top of the substrate. These remaining segments served as electrodes for *in-situ* four-point-probe resistance measurements (Agilent 4145B Semiconductor Parameter Analyzer) during NO exposure.

3. Results and discussion

3.1. Conductivity enhancement in PANI–PAAMPSA via redox cycling

To convert PANI–PAAMPSA films from their as-spun ES oxidation state to their fully-reduced LB oxidation state, films were exposed to a neat solution of hydrazine monohydrate possessing a vapor pressure of 5 mm Hg at room temperature. Specifically, PANI–PAAMPSA films were suspended inside sealed Petri dishes containing hydrazine monohydrate. Fig. 1 shows UV–vis/NIR absorption spectra for PANI–PAAMPSA films as a function of hydrazine monohydrate exposure time. Complete reduction is achieved near 10 s as evidenced by the complete suppression the polaron and polaronic shoulder features at 420 nm and 800 nm, respectively, associated with the ES state of PANI in the UV–vis/NIR spectra in Fig. 1.

In order to assess the influence of the reduction process on the structure of PANI–PAAMPSA films, AFM was performed on these films following exposure to hydrazine monohydrate of varying durations. Prior to AFM measurements, the samples were slowly dried for 1 h over each of a series of saturated salt solutions above which the relative humidity was iteratively lowered from 100% to 10% to prevent the formation of cracks during drying [19]. Fig. 2a shows an AFM micrograph obtained on a dried film that was chemically reduced by exposure to saturated hydrazine monohydrate vapors for 2 min. The particulate nature of the film is still clearly visible in terms of the periodic undulations on length scales of approximately 1.5 μm, in agreement with studies employing PANI template synthesized on 724 kg/mol PAAMPSA [13]. Relative to the RMS roughness of as-spun PANI–PAAMPSA films (62.4 nm), however, the surface of PANI–PAAMPSA following a two-minute reduction with hydrazine exposure is smoother (RMS roughness of 33.4 nm). Fig. 2b–d shows AFM micrographs obtained on dried PANI–PAAMPSA films that were reduced under hydrazine monohydrate vapors for 4, 8, and 10 min, respectively. These AFM micrographs reveal that the films become progressively smoother and exhibit less undulation upon prolonged exposure, reaching a minimum RMS roughness of 7.9 nm at 10 min. However, this trend does not continue on extended exposures as large portions of the film dewet from the underlying substrate. Fig. 2e quantifies the RMS roughness of PANI–PAAMPSA films as a function of hydrazine monohydrate exposure time. For reference, the dotted line imposed on the graph at 4.3 nm corresponds to the RMS roughness of a DCA-treated film, and it closely matches the RMS roughness of PANI–PAAMPSA that had been exposed to hydrazine monohydrate for 10 min [2]. It thus appears that structural relaxation to eliminate the particulate nature of PANI–PAAMPSA can be accomplished through both DCA treatment and exposure to hydrazine monohydrate vapor.

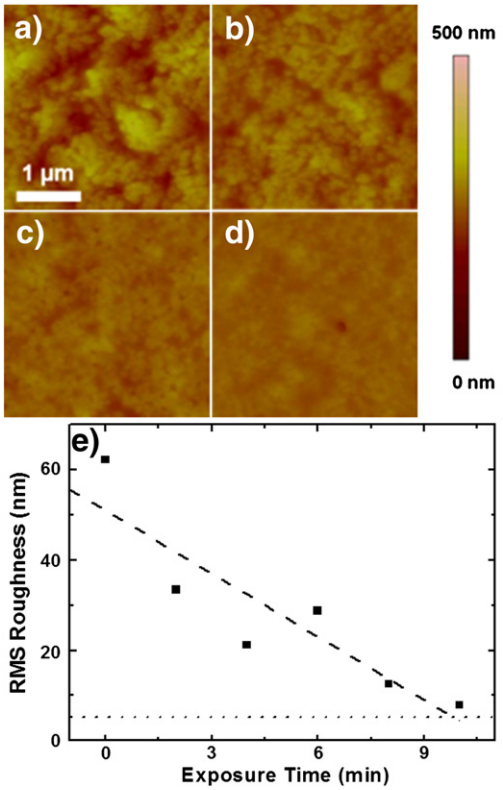

Fig. 2. AFM micrographs of the surfaces of dried PANI–PAAMPSA films following (a) 2-, (b) 4-, (c) 8-, and (d) 10-minute exposures to hydrazine monohydrate vapors. (e) Variations in the RMS roughness of PANI–PAAMPSA films are depicted as a function of hydrazine monohydrate exposure time. The dashed line represents a linear fit to the data, while the dotted line at an RMS value of 4.3 nm corresponds, for reference, to the roughness associated with PANI–PAAMPSA films that have been DCA-treated.

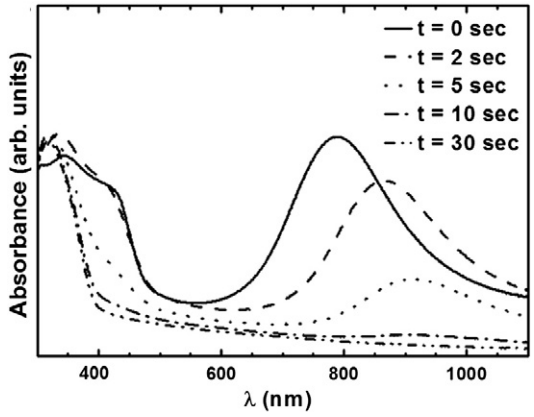

Fig. 1. UV–vis/NIR absorption spectra for a 450 nm-thick PANI–PAAMPSA film exposed to saturated hydrazine monohydrate vapors for varying durations.

Comparison of the UV–vis/NIR absorption spectra in Fig. 1 with the AFM micrographs shown in Fig. 2 suggests that chemical reduction and structural relaxation of PANI–PAAMPSA are separate processes that occur on different time scales. While UV–vis/NIR suggests that the complete reduction of PANI–PAAMPSA from its ES to its LB state takes place in less than 10 s, our AFM measurements indicate that structural rearrangement of PANI–PAAMPSA takes place over a much longer time scale of minutes. To deconvolute these processes, *in-situ* FTIR spectroscopy was employed in tandem with *in-situ* UV–vis/NIR spectroscopy. By maintaining identical film thicknesses, temporal resolutions, and hydrazine monohydrate exposure conditions, the measurements collected through these disparate techniques can be combined *via* synchronous correlation spectroscopy (SCS) and asynchronous correlation spectroscopy (ACS) [20,21]. Fig. 3a shows an SCS plot depicting UV–vis/NIR wavelengths on the horizontal axis and IR wavenumbers on the vertical axis. We observe that the IR absorbances near 1500 cm^{-1} and 1620 cm^{-1} correlate positively with the UV–vis/NIR absorbance at 330 nm. The feature at 330 nm is associated with the π–π* transition of PANI's benzenoid rings, [8,9] while the feature at 1500 cm^{-1} in the IR spectrum stems from C–H stretches of PANI's benzenoid rings [22]. Accordingly, the synchronicity of these

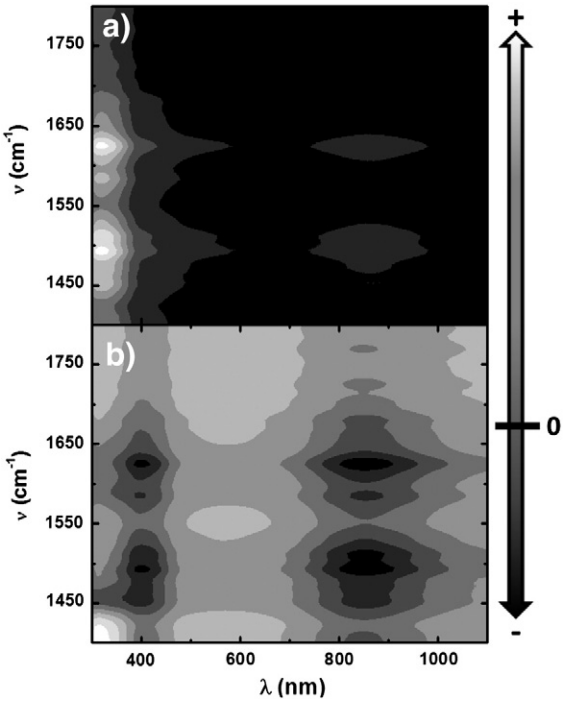

Fig. 3. (a) Synchronous and (b) asynchronous correlation spectroscopic plots comprising time-resolved UV–vis/NIR (horizontal axes) and FTIR (vertical axes) absorption spectra collected during the reduction of PANI–PAAMPSA by hydrazine monohydrate vapors under identical conditions. Colors above zero on the scale bar to the right indicate regions of positive correlation, while colors below zero indicate regions of negative correlation.

features is consistent with an increase in PANI's benzenoid content as it is reduced from ES to LB. The IR feature near 1620 cm^{-1} is not indicative of PANI's oxidation state, but stems from water uptake within the film as it is exposed to hydrazine monohydrate [23]. IR absorbance in these regions, alternatively, exhibits negative correlations with UV–vis/NIR absorbance at 420 nm associated with PANI's polaronic shoulder and at 800 nm associated with PANI's polaron. Given that the intensities associated with PANI's polaronic shoulder and polaron tend to decrease as PANI is converted from its ES oxidation state to LB, [8,9] the anti-synchronicity of these features is again consistent with the reduction of ES to LB with increasing water uptake. Fig. 3b shows an ACS plot describing the same dataset. As with the SCS counterpart, UV–vis/NIR wavelengths comprise the horizontal axis while IR wavenumbers comprise the vertical axis. In the ACS plot, we observe that the UV–vis/NIR absorbances at 420 nm and 800 nm exhibit negative correlations with the IR absorbances near 1500 cm^{-1} and 1620 cm^{-1}. Considering that these regions are also negatively correlated in the SCS plot, these negative ACS correlations indicate that PANI's polaronic shoulder (420 nm) and polaron (800 nm) undergo significant disruptions prior to increases in PANI–PAAMPSA's benzenoid (1500 cm^{-1}) character and the sample's moisture content (1620 cm^{-1}). Taken together, the SCS and ACS analysis quantifies what we noted in comparing Figs. 1 and 2. While PANI–PAAMPSA thin films undergo complete chemical reduction following 10 s of exposure to hydrazine monohydrate vapor, it is the subsequent exposure that allows the film to uptake moisture. This excess moisture in turn serves to relax the unlocked but otherwise glassy PAAMPSA chains, though at a rate much slower than that of chemical reduction (about 10 min according to Fig. 2e).

Having demonstrated that hydrazine monohydrate vapors can be employed in a humid environment to induce chemical reduction followed by structural relaxation of PANI–PAAMPSA, the question remains as to whether these films exhibit the same conductivity enhancements associated with DCA treatment when are they are oxidized back to the ES oxidation state. To oxidize PANI–PAAMPSA from chemically-reduced LB to ES, films were exposed to NO vapors that are generated according to Reaction (1). Changes in the optical and electrical properties of the films during exposure to NO were tracked by performing *in-situ* UV–vis/NIR and four-point-probe conductivity measurements.

Fig. 4a shows UV–vis/NIR spectra as a function of exposure time. The initial spectrum exhibits one significant feature at 330 nm, consistent with the LB oxidation state of PANI. A small shoulder near 420 nm is visible, and is due to intrinsic instability of the LB state at ambient conditions as LB partially oxidizes back to ES during the drying process [24]. Following 1500 s of exposure to NO, the film exhibits an absorption spectrum that possesses extensive polaron delocalization and intense absorption at NIR wavelengths, a quality that has previously been associated with highly conductive forms of PANI's ES state [2,25]. Additional exposure, however, results in oxidation beyond ES and towards PANI's fully-oxidized but electrically insulating pernigraniline base (PB) oxidation state.

The evolution of PANI–PAAMPSA's conductivity and absorbance at 1100 nm, determined through simultaneous *in-situ* four-point-probe and UV–vis/NIR measurements, respectively, are shown in Fig. 4b. For reference, the dotted line at 0.4 S/cm corresponds to the conductivity of freshly-spun PANI–PAAMPSA films, while the dashed line at 40 S/cm corresponds to the conductivity of DCA-treated PANI–PAAMPSA films [2]. A rapid increase in both conductivity and absorbance occurs near 1100 s, with conductivity peaking at 11.1 S/cm near 1450 s, and gradual decreasing through the duration of exposure. The rapid increase in PANI's conductivity following 1100 s of exposure stems from the onset of oxidation of LB, reaching the peak ES state at 1450 s; the gradual

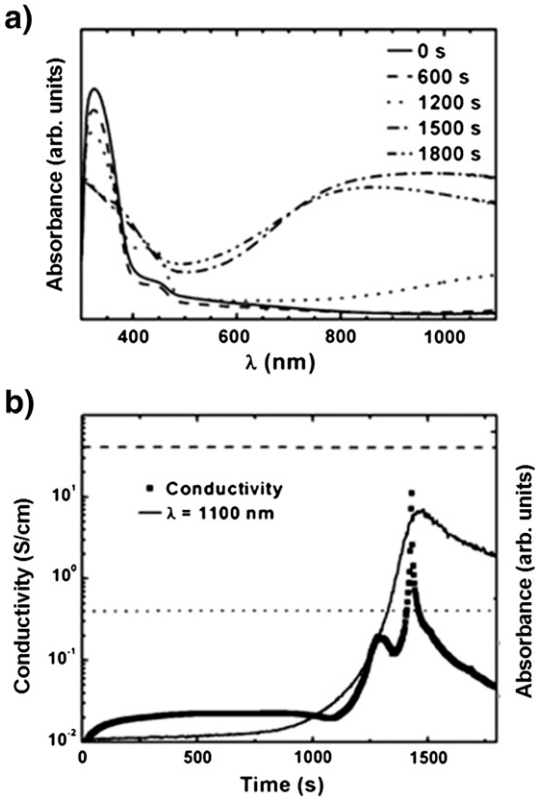

Fig. 4. (a) UV–vis/NIR absorption spectra collected *in-situ* during the oxidation of previously-reduced and dried PANI–PAAMPSA films under exposure to NO are shown as a function of time. (b) Conductivity and absorbance at 1100 nm, determined through simultaneous four-point-probe and UV–vis/NIR measurements, are shown as a function of exposure time during NO oxidation of previously-reduced and dried PANI–PAAMPSA films. The dotted line at a conductivity of 0.4 S/cm corresponds, for reference, to the initial conductivity of as-spun PANI–PAAMPSA, whereas the dashed line at a conductivity of 40 S/cm corresponds to the conductivity of DCA-treated PANI–PAAMPSA.

decrease at longer times reflects over-oxidation of PANI from ES to PB. Although this redox cycling process possesses the potential for over-oxidation, it conclusively confirms that the conductivity enhancements observed following DCA treatment are solely due to its ability to unlock the ionic interactions between PANI and PAAMPSA and impart dramatic structural change, and subsequently reestablish the ionic interactions upon its departure.

To demonstrate the versatility of this redox-cycling process in imparting conductivity enhancements to PANI–PAAMPSA films on any substrates, PANI–PAAMPSA spun-cast on poly(ethylene terephthalate), PET, substrates were patterned with a stencil and a moist cotton-tipped applicator and subjected to hydrazine monohydrate and NO exposures under conditions identical to those identified for films deposited on pre-patterned ITO substrates. An optical micrograph representing these PANI–PAAMPSA on PET samples is shown in the inset of Fig. 5. Rather than the *in-situ* four-point-probe conductivity measurements performed on patterned ITO substrates, two-point electrical measurements were performed by measuring the resistance between the nodes at the tops and bottoms of the serpentine pattern prior to and following redox cycling. As shown in Fig. 5, pristine PANI–PAAMPSA exhibits a cumulative resistance of 24 ± 4 MΩ over an aggregate distance of 9.6 cm. The same serpentine pattern after it has undergone redox cycling, alternatively, exhibits a cumulative resistance of 10 ± 5 MΩ over the same distance. Although the reduction in resistance is not as high as the conductivity enhancement seen in Fig. 4b, likely as a result of contact resistance and slight over-oxidation of PANI–PAAMPSA, redox cycling clearly induces significant enhancements without regard to substrate characteristics.

3.2. Redox cycling of PEDOT:PSS

Conductivity enhancement through solvent annealing with DCA has been established for both PANI–PAAMPSA and PEDOT:PSS, films comprising these two materials, however, exhibit dramatically different morphological changes during the process. The treatment is thereby speculated to operate *via* separate mechanisms on these two systems [2]. The conductivity enhancement for PANI–PAAMPSA has been shown to result from extensive structural changes within the film that are facilitated by neutralization of the ionic interactions between PANI and PAAMPSA, relaxation of PAAMPSA, and subsequent reassociation of the two species. As described here, this process can be induced along completely independent chemical redox routes yielding similar results, therefore robustly proving this three-stage mechanism as the method for improving the conductivity of PANI–PAAMPSA. Alternatively, conductivity enhancement in PEDOT:PSS is speculated to stem from the removal or disruption of an insulating PSS overlayer [15]. Given that PSS is not volatile, and thus impossible to remove through vapor annealing, PEDOT:PSS films were subjected to an identical set of experiments as those discussed above for PANI–PAAMPSA to delineate between the two mechanisms responsible for conductivity enhancement.

Fig. 6a shows time-resolved UV–vis/NIR absorption spectra obtained *in-situ* during the reduction of PEDOT:PSS under hydrazine monohydrate vapors. As the film is reduced, a large absorption peak emerges near 600 nm and the absorption in the NIR decreases; these trends are consistent with previous reports describing the reduction of PEDOT from its conductive, oxidized form to an insulating state in which the electrostatic interaction between PEDOT and PSS is significantly reduced [15,26–28]. Following exposure, there is no discernible difference in the morphology or RMS roughness of the film. This observation is different from that of PANI–PAAMPSA after hydrazine monohydrate exposure. Presuming the speculative mechanism for conductivity enhancement in PEDOT:PSS is valid, the lack of roughening following hydrazine monohydrate exposure should not be surprising given that PSS is non-volatile and that there is no solvent into which it can dissolve. Compared to solvent annealing in DCA, in which PSS is soluble, the PSS overlayer cannot be removed or significantly disrupted during

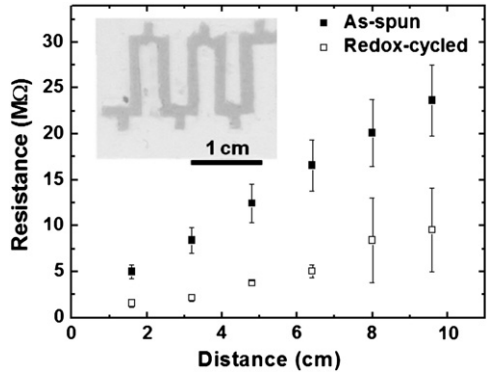

Fig. 5. Resistance is shown as a function of distance for the PANI–PAAMPSA pattern (■) prior to and (□) following redox-cycling, with error bars indicating the spread in resistance measured across a set of five samples. Inset shows an optical micrograph of a patterned PANI–PAAMPSA film deposited on PET substrates.

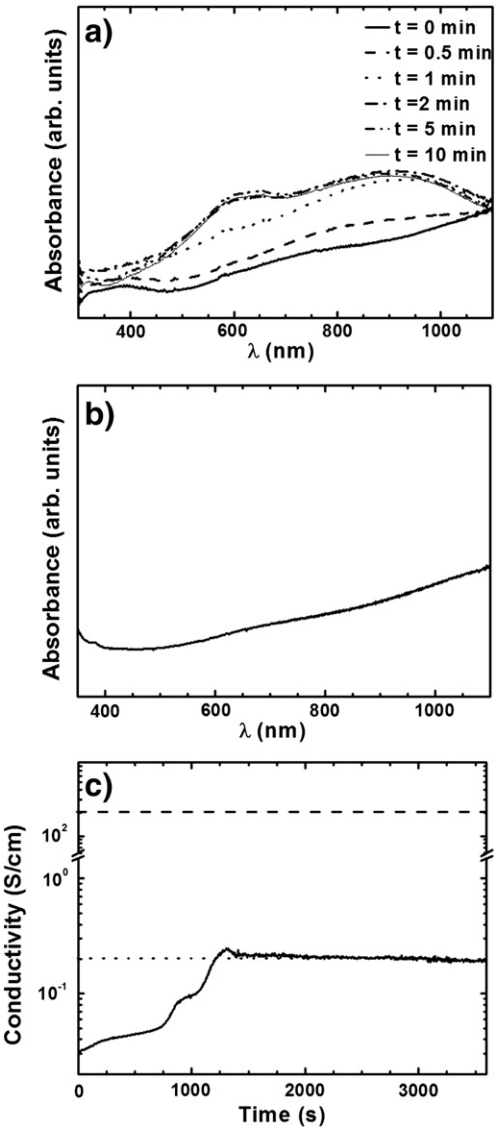

Fig. 6. UV–vis/NIR absorption spectra obtained (a) *in-situ* during the reduction of PEDOT:PSS under hydrazine monohydrate vapors and (b) following exposure to NO. (c) Conductivity of a previously-reduced PEDOT:PSS film, determined through *in-situ* four-point-probe measurements, is shown as a function of time during exposure to NO. The dotted line represents the initial conductivity of as-spun PEDOT:PSS, while the dashed line corresponds to the conductivity of DCA-treated PEDOT:PSS.

hydrazine monohydrate exposure. To determine whether the process of neutralizing the electrostatic association of PEDOT and PSS, and subsequently providing PSS the opportunity to relax in the presence of moisture, has any influence on the electrical properties of the film, *in-situ* UV–vis/NIR and four-point-probe conductivity measurements were obtained while a chemically-reduced PEDOT:PSS film was exposed to NO vapors. Fig. 6b shows the UV–vis/NIR absorption spectra of PEDOT:PSS obtained at the end of NO exposure and confirms that PEDOT has been returned from its reduced state to its initial oxidation state. Fig. 6c shows time-resolved conductivity measurements of the PEDOT:PSS film. The conductivity increases slowly and steadily at the onset of NO exposure; by 1200 s, the conductivity has returned to the value associated with freshly-spun PEDOT:PSS (0.2 S/cm), and it quickly plateaus for the duration of the exposure. Different from PANI–PAAMPSA, this experiment shows that redox cycling is only capable of switching PEDOT between its reduced and oxidized forms without imparting any observable structural change or conductivity enhancement. Accordingly, the mechanism by which DCA and other solvent-annealing techniques induce conductivity enhancements in PEDOT:PSS must differ significantly from that associated with DCA treatment of PANI–PAAMPSA. The underlying cause of this difference is not fully understood, but likely stems from intrinsic structural differences between PANI–PAAMPSA and PEDOT:PSS particles. In the former, conducting PANI is enriched on the exterior of the particle, [2,13] while in the latter, conducting PEDOT is enriched on the interior [3]. By relaxing the PAAMPSA-rich cores of PANI–PAAMPSA particles, rather than the PSS-rich corona of PEDOT:PSS particles, dramatic structural rearrangements are permitted.

4. Conclusions

By performing a combination of AFM, *in-situ* UV–vis/NIR spectroscopy, and *in-situ* four-point-probe conductivity measurements, the influence of redox cycling on the structural and electrical properties of PANI–PAAMPSA and PEDOT:PSS films was investigated. Redox cycling induces changes in the structure of PANI–PAAMPSA films; these changes are nearly identical to those observed following DCA treatment. Furthermore, these structural changes impart remarkably similar improvements in the electrical conductivity observed in the DCA treatment of PANI–PAAMPSA films.

The ability to realize these changes *via* chemical redox routes that are distinct from DCA treatment firmly corroborates a three-step sequence of (i) neutralizing PANI and PAAMPSA electrostatic interactions, (ii) permitting the otherwise-glassy PAAMPSA chains to relax, and (iii) stimulating the reassociation of the PANI–PAAMPSA complex as the dominant mechanism responsible for improving the electrical performance of the material. The inability of this three-step process to induce any changes in the properties of PEDOT:PSS films, alternatively, strongly suggests that the mechanism by which DCA imparts large conductivity enhancements is entirely different. This cause of the difference is not understood, but likely stems from opposing composition distribution of the conductive polymer within the respective particles.

Conductivity enhancement *via* redox chemical reactions possesses processing advantages compared to the previously-reported DCA treatment. DCA treatment, for instance, involves aggressively agitating films in a strong acid at 100 °C, followed by thermal annealing at 170 °C. As a consequence of these conditions, DCA treatment is limited to films deposited on rigid inorganic substrates, such as glass or silicon oxide, that can maintain structural integrity at elevated temperatures in a harsh acid [2]. Attempts to perform DCA treatment on PANI–PAAMPSA films deposited on polyethylene terephthalate (PET) substrates, for instance, immediately results in swelling and deformation of the substrates. As a consequence, DCA treatment presents formidable obstacles in terms of scalability and implementation in roll-to-toll fabrication processes. Structural relaxation through redox cycling, alternatively, proceeds *via* relatively-passive exposure to vapors comprising reducing and oxidizing agents at ambient conditions that involve no physical contact with liquid solvents. Although hydrazine monohydrate and NO were employed in this study, a broad range of reducing and oxidizing agents exists that should produce the same phenomena, provided that they possess appropriate reducing and oxidizing potentials. With care to avoid over-oxidation of PANI–PAAMPSA, this unique vapor-exposure process is amenable to films deposited on a much wider variety of substrates, and opens the door to realizing highly conductive PANI electrodes on plastic or paper for broad organic electronic applications.

Acknowledgment

This work was supported by the Beckman Foundation & NSF CAREER Award (DMR0735148). JT acknowledges the NIST-ARRA Measurement Science and Engineering Fellowship program. AFM images were collected at Princeton's Imaging and Analysis Center, supported by the Princeton Center for Complex Materials, an NSF MRSEC center.

References

[1] M. Angelopoulos, N. Patel, J.M. Shaw, N.C. Labianca, S.A. Rishton, J. Vac. Sci. Technol., B: Nanotechnol. Microelectron.: Mater., Process., Meas., Phenom. 11 (6) (1993) 2794.
[2] J.E. Yoo, K.S. Lee, A. Garcia, J. Tarver, E.D. Gomez, K. Baldwin, Y. Sun, H. Meng, T.-Q. Nguyen, Y.-L. Loo, Proc. Natl. Acad. Sci. U. S. A. 107 (13) (2010) 5712.
[3] S. Kirchmeyer, K. Reuter, J. Mater. Chem. 15 (21) (2005) 2077.
[4] J. Tarver, J.E. Yoo, Y.-L. Loo, in: G.P. Wiederrecht (Ed.), Handbook of Nanoscale Optics and Electronics, Academic Press, 2010, p. 107.
[5] J. Tarver, Y.-L. Loo, Chem. Mater. 23 (19) (2011) 4402.
[6] D.M. DeLongchamp, P.T. Hammond, Chromogenic Phenomena in Polymers, vol. 888, American Chemical Society, 2004. 18.
[7] H. Hu, L. Hechavarria, J. Campos, Solid State Ionics 161 (1–2) (2003) 165.
[8] J. Tarver, J.E. Yoo, T.J. Dennes, J. Schwartz, Y.-L. Loo, Chem. Mater. 21 (2) (2008) 280.
[9] J. Tarver, J.E. Yoo, Y.-L. Loo, Chem. Mater. 22 (7) (2010) 2333.
[10] Y.-L. Loo, I. McCulloch, MRS Bull. 33 (7) (2008) 653.
[11] J.E. Yoo, T.L. Bucholz, S. Jung, Y.-L. Loo, J. Mater. Chem. 18 (26) (2008) 3129.
[12] J.E. Yoo, J.L. Cross, T.L. Bucholz, K.S. Lee, M.P. Espe, Y.-L. Loo, J. Mater. Chem. 17 (13) (2007) 1268.
[13] J.E. Yoo, W.P. Krekelberg, Y. Sun, J.D. Tarver, T.M. Truskett, Y.-L. Loo, Chem. Mater. 21 (9) (2009) 1948.
[14] X. Crispin, S. Marciniak, W. Osikowicz, G. Zotti, A.W.D. van der Gon, F. Louwet, M. Fahlman, L. Groenendaal, F. De Schryver, W.R. Salaneck, J. Polym. Sci. B Polym. Phys. 41 (21) (2003) 2561.
[15] S.K.M. Jönsson, J. Birgerson, X. Crispin, G. Greczynski, W. Osikowicz, A.W. Denier van der Gon, W.R. Salaneck, M. Fahlman, Synth. Met. 139 (1) (2003) 1.
[16] J.Y. Kim, J.H. Jung, D.E. Lee, J. Joo, Synth. Met. 126 (2–3) (2002) 311.
[17] J. Ouyang, C.W. Chu, F.C. Chen, Q. Xu, Y. Yang, Adv. Funct. Mater. 15 (2) (2005) 203.
[18] J. Ouyang, Q. Xu, C.-W. Chu, Y. Yang, G. Li, J. Shinar, Polymer 45 (25) (2004) 8443.
[19] L.B. Rockland, Anal. Chem. 32 (10) (1960) 1375.
[20] I. Noda, Appl. Spectrosc. 47 (9) (1993) 1329.
[21] I. Noda, A.E. Dowrey, C. Marcott, G.M. Story, Y. Ozaki, Appl. Spectrosc. 54 (7) (2000) 236A.
[22] Y. Sun, A.G. MacDiarmid, A.J. Epstein, J. Chem. Soc. Chem. Commun. 7 (1990) 529.
[23] D.R. Lide, CRC Handbook of Chemistry and Physics, CRC Press, Boca Raton, FL, 2012.
[24] K.G. Neoh, E.T. Kang, K.L. Tan, J. Polym. Sci. B Polym. Phys. 31 (4) (1993) 395.
[25] A.G. MacDiarmid, A.J. Epstein, Synth. Met. 65 (2–3) (1994) 103.
[26] A.A. Argun, A. Cirpan, J.R. Reynolds, Adv. Mater. 15 (16) (2003) 1338.
[27] S. Garreau, G. Louarn, J.P. Buisson, G. Froyer, S. Lefrant, Macromolecules 32 (20) (1999) 6807.
[28] T. Johansson, L.A.A. Pettersson, O. Inganäs, Synth. Met. 129 (3) (2002) 269.